Biomedical Microdevices 7:1, 59–69, 2005

Drug-Delivery Micro/Nanotechnology Section:

Section Editor: Dr. Tejal Desai

Microdialysis Microneedles for Continuous Medical Monitoring

Jeffrey D. Zahn,[*,1,2,4] *David Trebotich,*[1,3] *and Dorian Liepmann*[1,2,3]

[1]*Berkeley Sensor and Actuator Center, University of California, Berkeley, 497 Cory Hall, Berkeley, CA 94720-1774, USA*
[2]*Department of Bioengineering, University of California, Berkeley, 459 Evans Hall, Berkeley, CA 94720-1762, USA*
[3]*Department of Mechanical Engineering, University of California, Berkeley. Berkeley, CA 94720-1740, USA*
[4]*Department of Bioengineering, The Pennsylvania State University, University Park, PA 16802, USA*
E-mail: jdz10@psu.edu

Abstract. **Enzyme based biosensors suffer from loss of activity and sensitivity through a variety of processes. One major reason for the loss is through large molecular weight proteins settling onto the sensor and affecting sensor signal stability and disrupting enzyme function. One way to minimize loss of sensor activity is to filter out large molecular weight compounds before sensing small biochemicals such as glucose. A novel microdialysis microneedle is introduced that is capable of excluding large MW compounds based on size. Preliminary experimental evidence of membrane permeability is shown, as well as diffusion and permeability modeling. Microdialysis microneedles present an attractive first step towards decreasing size, patient discomfort and energy consumption of portable medical monitors over existing technologies.**

Key Words. **microneedle, microdialysis, porous polysilicon, microshell**

1. Introduction

Microneedles have emerged as promising microfabricated devices that have biological and medical applications (Zahn et al., 2000; Talbot and Pisano, 1998; Lin et al., 1993; Henry et al., 1998; Brazzle et al., 1999; Lebouitz, 1998). Small needles are desirable because they reduce insertion pain and tissue damage in the patient and can be integrated into a variety of devices. They may be used for parallel fluid sampling, analysis, and drug delivery. Microfabricated needles are especially attractive because they may be fabricated with great precision. This precision can provide systems for which penetration depth can be controlled and drug delivery may be enhanced by targeting specific tissue types below the skin (Liepmann et al., 1997, 1999). For example, this targeting is important for interstitial fluid sampling, where shallow needle penetration makes it highly unlikely for blood vessels to be severed to corrupt sampling.

When microneedles are used to sample interstitial fluid, biosensor stability and lifetime can be extended if metabolites are filtered through a microdialysis needle before fluid is moved onto the sensor. Protein adsorption onto a sensor seriously affects the stability and lifetime of a sensor. For this reason, many commercial enzyme based biosensors (e.g. glucose sensors) are single-use systems. In order to accurately monitor biochemical concentrations, single-use sensors must be calibrated against a standard solution prior to use.

Another approach is to protect the sensors from protein adsorption and subsequent loss of enzyme activity by using diffusion membranes. Even with these precautions, sensors are only reliable within 10–15% of the true chemical concentration. Protein adsorption is a critical bottleneck to the development of continuous electrochemical monitors.

Diffusion membranes are also susceptible to protein adsorption, which affect the mass transfer characteristics of the sensor. Because electrochemical sensors are usually operated in a diffusion limiting regime, a decrease in mass transfer rate will lead to a decrease in sensor signal. Free enzymes in solution can catalyze side reactions where the products of these reactions increase the noise and false signal at the sensor. Free proteins can also disrupt enzyme function so reactions are not catalyzed and no signal is detected by the sensor.

For example, a glucose sensor uses the enzyme glucose oxidase to catalyze the reaction between glucose and oxygen to produce gluconic acid and hydrogen peroxide (H_2O_2). The H_2O_2 is subsequently oxidized at a platinum electrode to generate a current which is directly

*Corresponding author.

proportional to the glucose concentration (Lambrechts and Sansen, 1992). If there is a loss of enzyme activity then H_2O_2 is not produced and the signal at the sensor will be lower than the actual glucose concentration. Removing free protein from biological solutions before sensing metabolites will help increase sensor accuracy and lifetime.

Current microdialysis needles have a very large bore, consume a large amount of fluid, and are uncomfortable during insertion and prolonged wear. They also require a serial assembly in which a dialysis membrane is inserted and bound into an 18-gauge needle. There are also dialysis type needles with integrated glucose sensors in the bore of a stainless steel needle which require even more assembly (Lambrechts and Sansen, 1992). Dialysis fluid flows at 1 μl/min with a 2 minute equilibrium time (Towe and Pizziconi, 1997). In addition, the large needle is inserted directly into the bloodstream which causes discomfort.

A microfabricated dialysis microneedle (Figure 1) has been developed which is permeable to small molecular

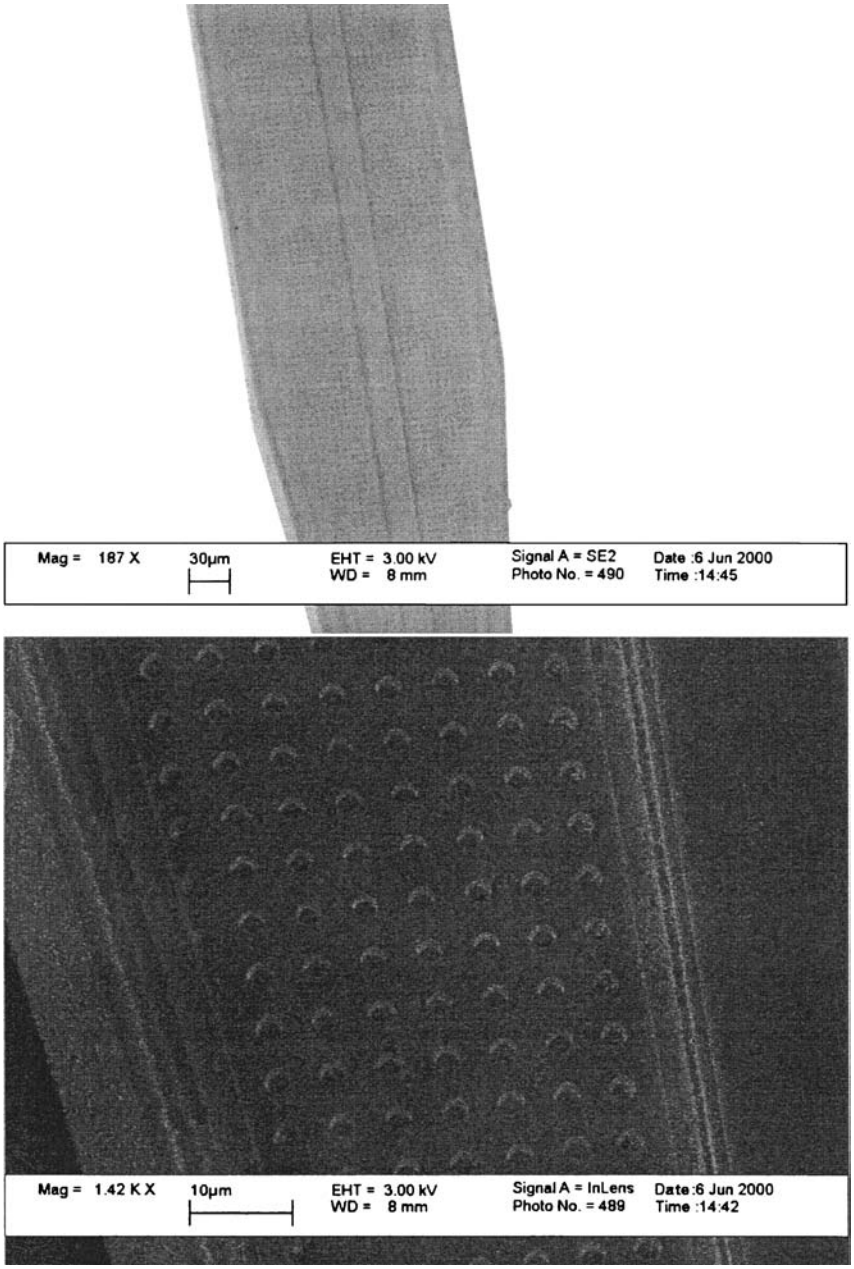

Fig. 1. *(Top) SEM picture of a microdialysis microneedle. (Bottom) Closeup of the microdialysis membrane. The arrayed dots on the needle represent 2 μm features defining the dialysis membrane.*

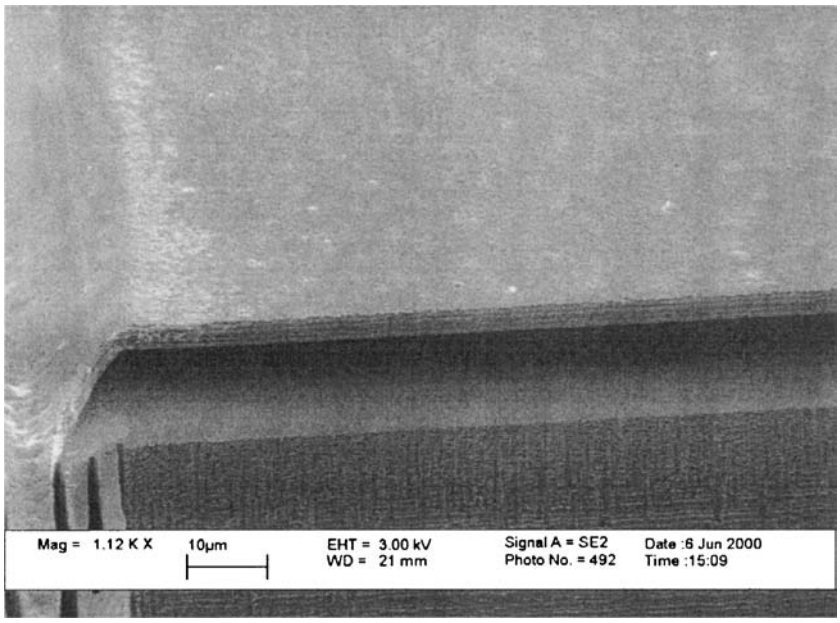

Fig. 2. *The back of a microneedle showing the microshell fabricated on top of the substrate. A sacrificial oxide spacer defines the 10 μm channel height before it is removed in hydrofluoric acid.*

weight (MW) molecules, yet excludes large MW compounds such as proteins. This microneedle, compared to existing technologies, is designed to be an order of magnitude smaller in almost all characteristics, while meeting the same performance criteria. It is also fabricated *in situ* so no assembly is necessary. In addition, the needle can also easily be integrated with planar electrochemical sensors either by batch transfer or direct fabrication on the needle so no serial assembly with sensors would be required. The fluid channel is 10 μm high (Figure 2). This dramatic miniaturization results in smaller sample volumes, more rapid diffusion equilibrium of analytes between interstitial fluid and dialysis fluid, and a lower overall power to operate the system. The needle protrudes just below the stratum corneum (the topmost layer of the skin), and analyte concentrations equilibrate between the interstitial fluid and dialysis fluid. The concentration of many analytes in interstitial fluid, including glucose, is strongly correlated with blood concentrations, while the superficial protrusion of the needle under the skin minimizes patient discomfort.

Microdialysis needles are based upon the direct separation of large MW from small analytes through the dialysis membrane. Such approaches have been used for immunoisolation of cells in microfabricated biocapsules (Desai et al., 1998, 1999). However, these biocapsules still allow the diffusion of smaller proteins such as insulin. The microdialysis membranes presented here are expected to have a size exclusion property, so that even if a smaller molecular weight protein enters the diffusion channel, its mobility will be retarded by the geometry of the channel.

2. Fabrication

Needles are fabricated as a polysilicon microshell on top of a silicon substrate (Lin et al., 1993; Lebouitz, 1998) using a silicon on insulator (SOI) device layer as a mechanical support (Figure 3). Two permeable needle designs have been fabricated. The first is a diffusion membrane fabricated using a layered polysilicon sandwich with a thin thermally grown oxide (10–50 nm) between the layers, and appropriate etch access holes (Desai et al., 1998, 1999). A second microdialysis membrane takes advantage of permeable polysilicon. Lebouitz (1998) used this technology for vacuum encapsulation of resonators. Permeable polysilicon has pore defects (5–20 nm wide) which allow small molecules to permeate between the polysilicon grains.

To fabricate the diffusion membrane 10 μm of sacrificial low temperature oxide (LTO) (450°C, 90 sccm O_2, 60 sccm SiH_4, and 450°C) is first deposited onto a 50 μm thick device layer of a SOI wafer by low pressure chemical vapor deposition (LPCVD). The LTO is annealed at 900°C in a nitrogen atmosphere, masked and etched (CF_4 plasma) to define the flow passage. Then 2–3 μm of polysilicon is deposited (100 sccm SiH_4, 300 mTorr, 580°C) to define the microshell. The polysilicon is annealed in a nitrogen atmosphere at 900°C to ensure a tensile stress in the film. The polysilicon is masked with 2 μm open holes and etched in a Cl_2 plasma. The polysilicon is then oxidized in a dry oxygen atmosphere at 900°C to grow 10–50 nm of thermal oxide which defines the diffusion passage.

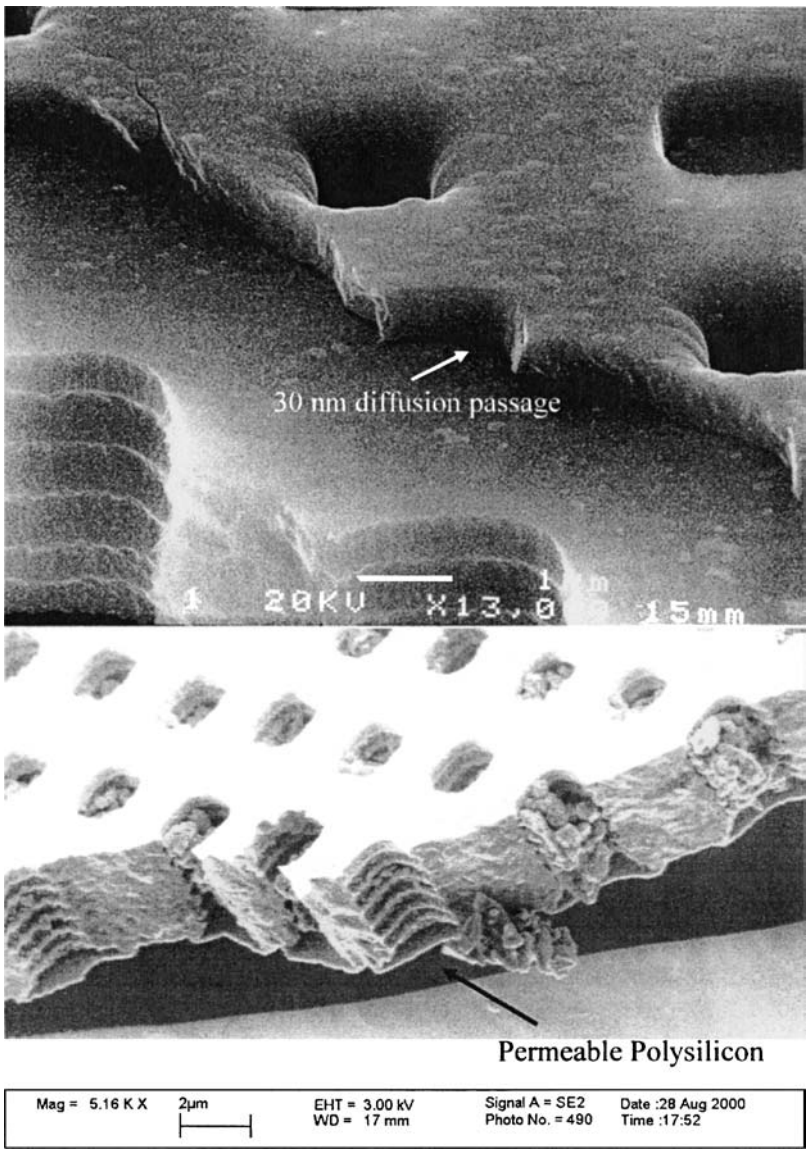

Fig. 3. *(Top) Diffusion channel dialysis membrane. A thin (30 nm) opening can be seen between the polysilicon layers. In addition, when the layers were fractured they delaminated and fractured at different points indicating the layers are separate. (Bottom) Permeable polysilicon membrane. The permeable polysilicon layer can be seen at the bottom of the trenches.*

200 nm of polysilicon is then deposited and annealed as before. This thin polysilicon layer is masked, etched and adhesion anchors are defined by etching the thin oxide in hydrofluoric acid (HF). A 500 nm polysilicon layer is deposited, annealed, masked and etched to intersect with the thinly grown oxide. The needle shape is then patterned and the needle is etched down to the buried oxide of the SOI wafer in a surface technologies systems (STS) deep reactive ion etcher (DRIE). The needles are released in concentrated hydrofluoric acid for several hours until all the sacrificial oxide is removed. This release also opens up the diffusion channel (Figure 4). Since all the polysilicon has been annealed to be tensile, there should be no buckling between layers which could pinch off the channels.

The permeable polysilicon membrane is fabricated similarly to the diffusion membrane (Figure 5). First a 10 μm LTO is deposited onto a SOI wafer. Then 2–3 μm of polysilicon is deposited, annealed, patterned and etched. 120 nm of permeable polysilicon is then deposited at 597°C, 125 sccm SiH_4, and 555 mTorr (Figure 6). The needle shape is patterned and cut out using the STS. The needle is then released in HF for several hours.

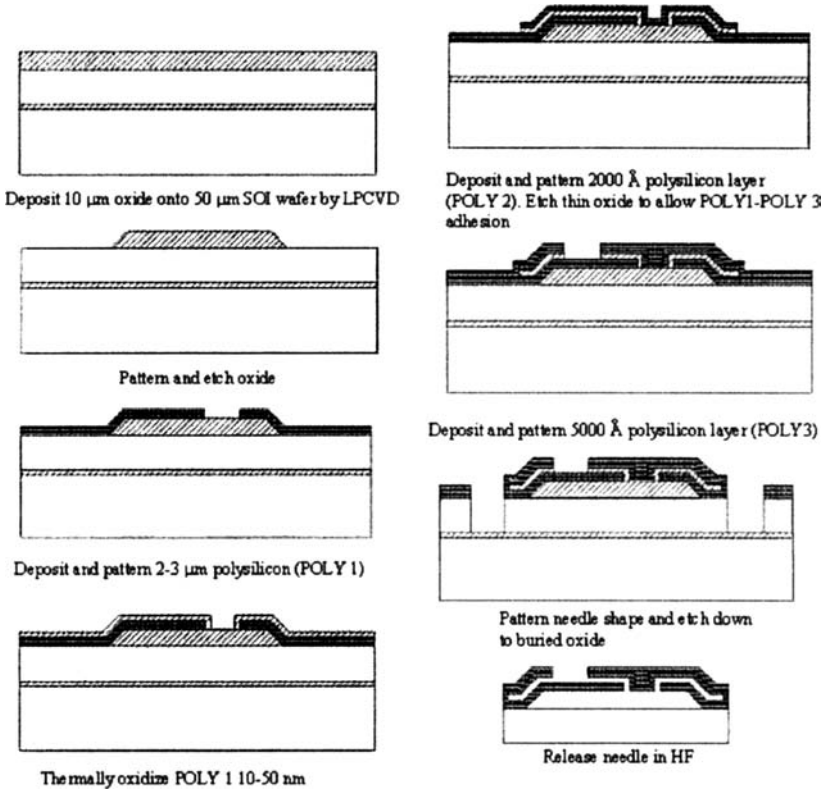

Fig. 4. *Fabrication details of the microdialysis membrane. The microshell is formed over a sacrificial oxide spacer layer. Several polysilicon layers are sandwiched around a thin sacrificial oxide which defines the diffusion channel. Appropriate access holes are etched into the polysilicon layers to allow small MW molecules to permeate across the membrane.*

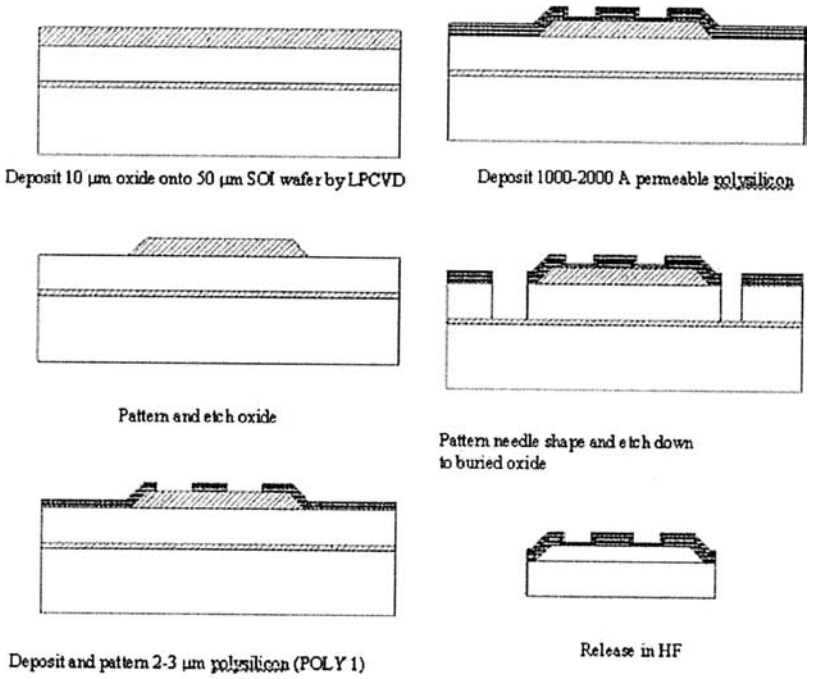

Fig. 5. *Fabrication details of the permeable polysilicon membrane. Windows are etched into polysilicon microshell and a thin layer of permeable polysilicon is deposited. The permeable polysilicon has 5–20 nm pore defects which should allow small molecules to permeate.*

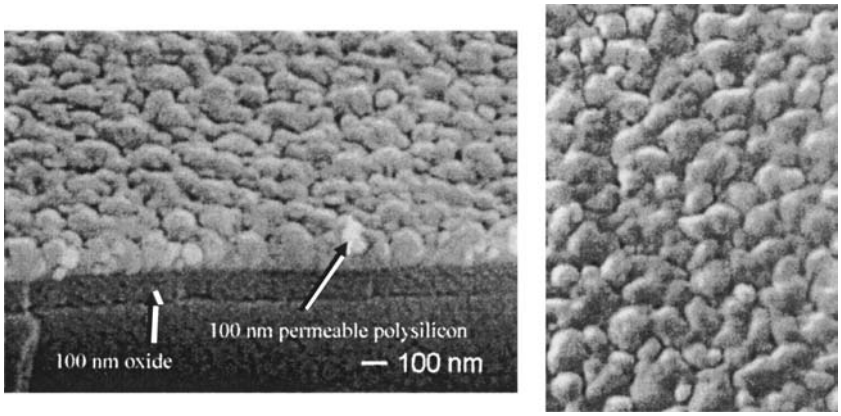

Fig. 6. (Left) 100 nm of permeable polysilicon on top of 100 nm of silicon dioxide. (Right) Top view of the permeable polysilicon. The polysilicon is permeable because of the large grain size (∼150 nm) with defects at the grain boundaries which can be easily discerned.

3. Theory

3.1. Fluid flow

For fully developed flow in the laminar regime the x-directed velocity profile in a rectangular duct with y and z cross section is given by

$$\begin{aligned} v_x = {} & \frac{16a^2}{\mu\pi^3}\left(-\frac{dP}{dx}\right)\sum_{i=1,3,5\ldots}^{\infty}(-1)^{(i-1)/2} \\ & \times\left[1-\frac{\cosh(i\pi z/2a)}{\cosh(i\pi b/2a)}\right]\frac{\cos(i\pi y/2a)}{i^3} \\ & -a \le y \le a \\ & -b \le z \le b \end{aligned} \tag{1}$$

where $2a$ is the height of one of the walls, $2b$ is the width of the other wall, P is the pressure and μ is the viscosity of the solution. Integrating this profile across y and z gives the average flow rate, Q as

$$\begin{aligned} Q = {} & \frac{4ba^3}{3\mu}\left(-\frac{dP}{dx}\right)\left[1-\frac{192a}{\pi^5 b}\right. \\ & \left.\sum_{i=1,3,5\ldots}^{\infty}\frac{\tanh(i\pi b/2a)}{i^5}\right] \end{aligned} \tag{2}$$

The average velocity, U, is $Q/(4ab)$. Microdialysis needles have a 65 μm wide passage and with a height of 10 μm. This may be approximated by plane poiseulle flow.

$$v_x = \frac{a^2}{2\mu}\left(-\frac{dP}{dx}\right)\left[1-\left(\frac{y}{a}\right)^2\right] \tag{3}$$

Integrating across y and z gives

$$Q = \frac{4ba^3}{3\mu}\left(-\frac{dP}{dx}\right) \tag{4}$$

Please note that (equations (3) and (4)) also assume a height of $2a$ and a width of $2b$. Comparing (equations (2) and (4)) using the fabricated channel dimensions shows the flow resistance to be in agreement within 10 percent.

3.2. Mass transfer in the microchannel

In order to describe the mass transfer characteristics in the channel Fick's second law for single component diffusion is considered.

$$\frac{\partial C}{\partial t} + \bar{u}\cdot\bar{\nabla}C = D\bar{\nabla}^2 C \tag{5}$$

where C is the concentration and D is the diffusivity of the component of interest. For small molecules such as glucose D is assumed to be 10^{-9} m^2/sec. If 1-dimensional unsteady diffusion is assumed, then (equation (5)) simplifies to

$$\frac{\partial C}{\partial t} = D\frac{\partial^2 C}{\partial y^2} \tag{6}$$

This can be easily solved by separation of variables with the boundary conditions $C = C_O$ at $y = 0$, $t \neq 0$, a no pentration boundary condition, $\partial C/\partial y = 0$ at $y = 2a$ (the height of the wall) for all times, and the initial condition that $C = 0$ everywhere at $t = 0$, as

$$\begin{aligned} C = C_O\Bigg[1 - {} & \sum_{i=1,3,5\ldots}^{\infty}\frac{4}{i\pi}\sin\left(\frac{i\pi y}{4a}\right) \\ & \times \mathrm{Exp}\left(-\frac{(i\pi)^2 Dt}{16a^2}\right)\Bigg]. \end{aligned} \tag{7}$$

If diffusion out of the needle into the ambient is considered, then the needle can modeled as a constant source diffusing into a semi-infinite medium. The diffusion equation can be solved by a similarity solution

$$C = C_O\left[1-\mathrm{erf}\left(\frac{y}{\sqrt{4Dt}}\right)\right]. \tag{8}$$

If forced convection from fluid flow in the microchannel is considered, then computational methods must be employed to find the time varying concentration profile with coupled fluid flow.

3.3. Membrane permeability

The largest barrier to mass transfer is the dialysis membrane. Since the pore sizes are much larger than the molecules of interest we can define permeability as

$$P_n = \frac{Dkp}{dT} \tag{9}$$

where k is a partition coefficient (assumed to be 1), p is the porosity or volume fraction of pores versus total membrane volume, and T is the tortuosity of the membrane because the diffusion distance is larger than the thickness of the membrane. For the diffusion channel membrane described with a 30 nm diffusion channel $T = 2$ and $p = 0.016$.

The time for such a membrane to come to equilibrium is therefore approximated by compartment diffusion as

$$\frac{V}{A_m P_n} = \frac{2a}{P_n} \tag{10}$$

where V is the volume of the needle, and A_m is the area of the membrane for diffusion. This expression becomes the height of the flow passage divided by the permeability of the membrane.

The dialysis membranes are designed to exclude large molecules based on size. However, many proteins may be less than 30 nm in radius. They should be diluted by a size exclusion effect where steric hindrances (the molecules being the same order of magnitude in size as the flow passages and therefore are retarded by the pores) will slow proteins migration through the thin pores.

The diffusion coefficient for a large component n in a pore can be defined as

$$D_n^* = F(a/r)D_n \tag{11}$$

where $F(a/r)$ is the centeline approximation as described in Desai et al. (1998)

$$F(a/r) \approx 1 - 2.1044(a/r) + 2.089(a/r)^3 - 0.948(a/r)^5 \quad a/r < 0.4 \tag{12}$$

and D_n is approximated by the Stokes-Einstein relation

$$D_n = \frac{kT}{6\pi a\mu} \propto M^{-1/3} \tag{13}$$

where M is the molecular weight of the molecule. As the molecular weight of a molecule increases, its diffusion coefficient is smaller causing slower migration.

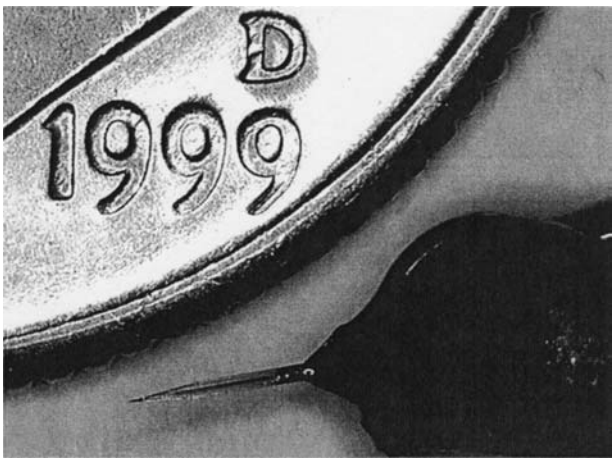

Fig. 7. *Packaged microneedle next to a dime for size comparison.*

4. Experimental Apparatus

To test the permeability of microdialysis microneedles, a concentrated fluorescein solution was visualized diffusing out of the needles. The needle was packaged by placing its two ends (the flow passage is U shaped) in polyimide tubing. The tubing is then sealed using a two part epoxy (Figure 7). Once the epoxy is dried, flexible tubing is placed inside the polyimide tubing and sealed using heat shrink tubing. A stainless steel needle is attached to the tubing and dye solution is infused through the needle at varying flow rates. The dye is visualized on a Olympus IX70 microscope with a mercury lamp light source.

5. Results and Discussion

In order to predict the effectiveness of a microdialysis needle, the mass transfer characteristics have been modeled in relevant medical situations. Since one of the largest applications of electrochemical sensors is for diabetics most of the modeling is done assuming glucose is diffusing into the needle. Therefore, it is assumed that the needle is bathed in interstial fluid with a constant concentration source of glucose in the physiological range (5 mM).

Membrane permeation has been analyzed. Equation (10) predicts that in a channel with a height of 10 μm, the microdialysis membrane should come to equilibrium in 2.5 seconds. In addition, as shown in Figure 8, equation (7) predicts that the dialysis solution in the channel will come to equilibrium in 0.3 seconds if a one dimensional diffusion solution is assumed. However, the largest resistance to mass transfer is the dialysis membrane and not free diffusion of small molecules into dialysis fluid. An upper time bound for the fluid in the needle to come to equilibrium with the

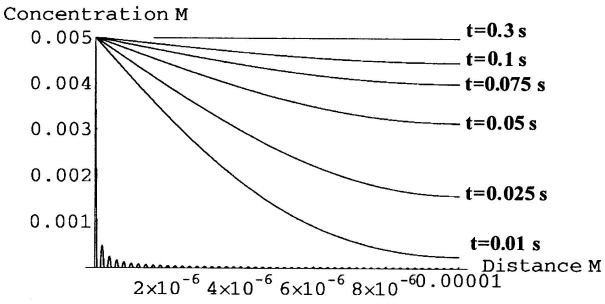

Fig. 8. Theoretical concentration profile of glucose from a 5 mM constant source. The diffusion constant is assumed to be 10^{-9} m^2/s for small molecules. The diffusion is in the y direction.

outside may be estimated by defining a perturbed diffusivity $D' = Dp/T \cdot D'$ for a small molecule such as glucose through the microdialysis membrane is 125 times smaller than its diffusity in water (10^{-9} m^2/s). Solving equation (7) by substituting in D' predicts that the channel will come to equilibrium in 15 seconds. This is the maximum time needed for fluid a 10 μm high channel to come to equilibrium with the dialysis membrane on top of it.

If it is assumed that plane poiseuille flow equation (3) is dominating the flow pattern in the channel, equation (5) can be computationally solved in 2 dimensions (Figure 9). The solution to the diffusion equation is generated using a computational fluid dynamics package (CFD-Ace, CFD Research Corp.) which accounts for the coupling of the flow profile with the concentration gradient. The fluid is assumed to be moving through the needle at 1 nl/s. 300 μm down the channel, after the entrance region, the solution to equation (5) in 2 dimensions is very similar to equation (7), the one dimensional diffusion solution. There is no concentration gradient in the x direction, only in y.

The two-dimensional solution to equation (5) has also been applied to determine the time to equilibrium through the combined dialysis membrane and flow channel (Figure 10). The 2 μm membrane is assumed to have diffusivity D' as discussed earlier. Again, 300 μm down the channel in the x direction, the solution becomes essentially a one-dimensional diffusion problem. In addition, it takes about 15 seconds for the channel to come to equilibrium with a 1 nl/s flow rate.

Finally, the situation in which material diffuses from 30 nm pores spaced 2 μm apart is considered. As shown in Figure 11, material diffuses out of the pores in both the x and y direction. Thus, there is a longer and more complicated transient period in which material diffuses into the channel. However, the gradient in the x direction disappears as material has diffuses in the x direction. The material then diffuses into the channel. The diffusion progresses more slowly than previously modeled, since there is no longer a constant source boundary condition and the

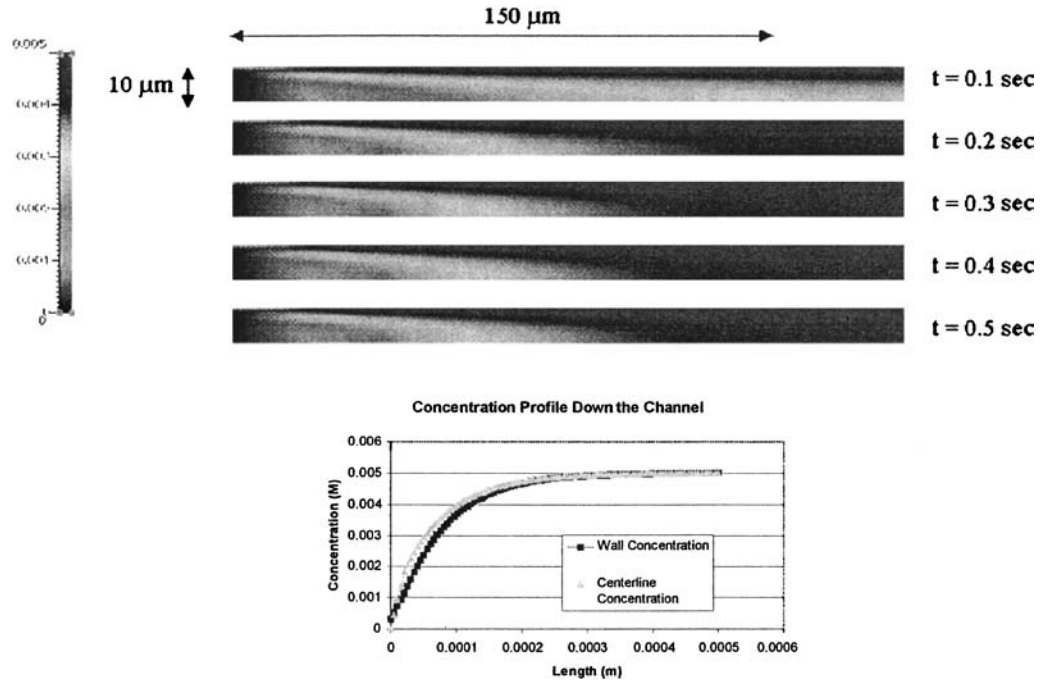

Fig. 9. Calculated 2-dimensional concentration profile from a constant source with parabolic fluid low at 1 nl/s. The concentration equilibrates down the channel in less than 1 second.

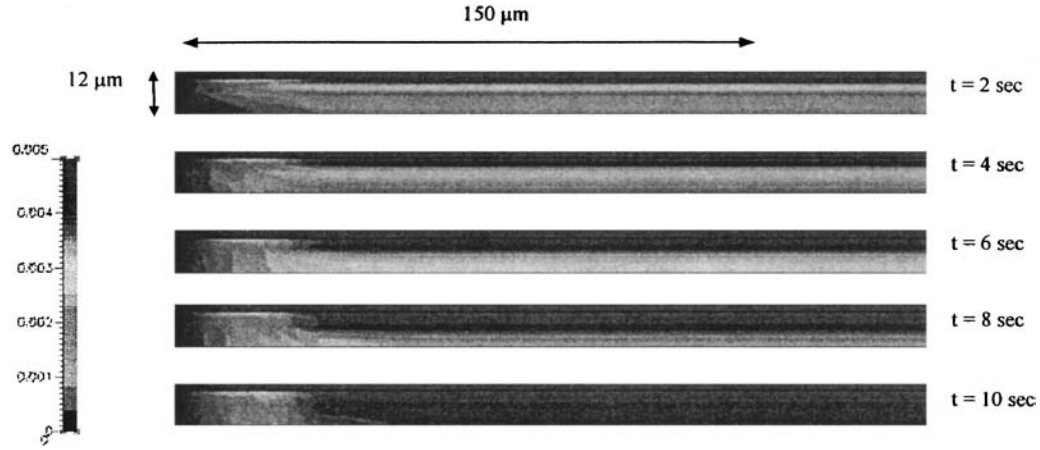

Fig. 10. *Calculated 2 dimensional diffusion from a constant source with parabolic fluid flow at 1 nl/s. The 2 µm microdialysis membrane is on the top of the channel creating a longer transient to equilibrium than is predicted without the membrane. The system stills comes to equilibrium in about 15 seconds.*

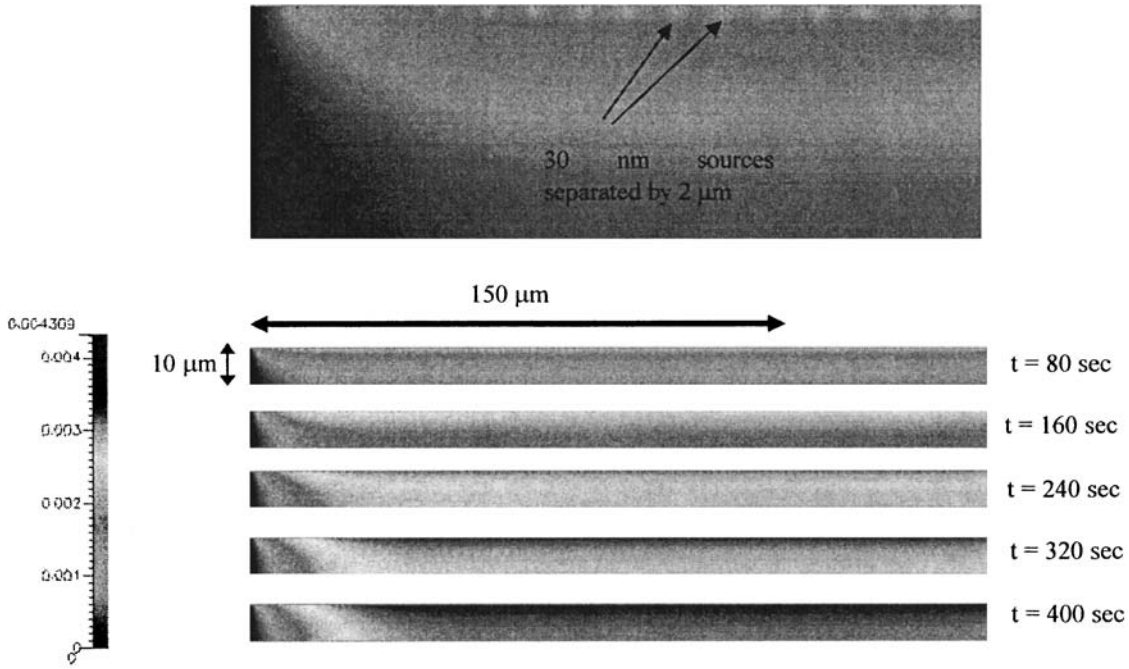

Fig. 11. *(Top) Close up of 30 nm sources at the channel entrance. (Bottom) Calculated 2 dimensional diffusion from the 30 nm sources with parabolic fluid flow at 1 nl/s. The discrete sources allow less mass flux into the channel creating a longer transient to equilibrium than is predicted from a constant source boundary condition. The system still comes to equilibrium in about 500 seconds.*

area of the pores is only 1.5% of the total surface area of the membrane.

In order to visualize that the diffusion membrane does in fact allow mass transfer across it, fluorescein dye (MW 322) has been visualized diffusing from the needle. These experiments were performed on diffusion passage type microneedles. First, dye was allowed to come to equilibrium with a droplet of water on the surface of the needle through the membrane (Figure 12). The dye can be seen on the outside of the needle and emerging from the needle. Next, the needle was submerged in water and dye was infused at a rate of 10 nl/s and fluorescence profiles were visualized as dye diffused out of and away from the needle (Figure 13). The actual fluorescein concentration could not be determined since the dye is continuously diffusing from the surface of the needle and being diluted in the surrounding water. However, the concentration is expected to be linearly related to the

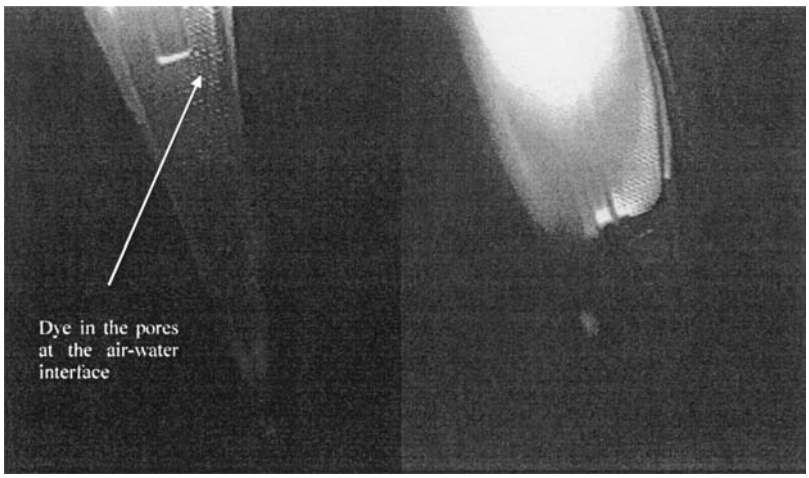

Fig. 12. (Left) Fluorescent dye emerging from pores on the needle tip. (Right) Fluorescent dye in equilibrium with a water droplet on the needle. The pores can be seen as small dots on the needle surface.

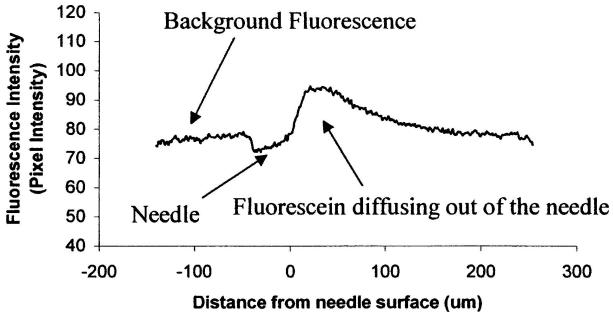

Fig. 13. Fluorescence signal as dye diffuses out of a needle. The low signal indicates the side of the needle, and the dye flux is from left to right beginning at the needle surface. The fluorescence brightness (0–255) is directly proportional to dye concentration in solution.

pixel intensity value. The fluorescence profile diffusing out of the needle follows the error function profile predicted in equation (8). These visualizations show that the needle microdialysis membranes will allow mass to permeate.

Large MW proteins are expected to be selectively excluded from the microneedles. In Desai et al. (1997, 1998) and co-workers were able to show immunoisolation through similarly sized pores. This implies that a 150 kDa antibody cannot permeate through a pore. However, Desai and co-workers were also able to see insulin (6 kDa) diffuse through the pores. However, the fluid was not a flow through system as in the microneedle. Thus, large proteins should be selectively excluded from permeating the microdialysis membrane since they cannot fit inside the small channels. Smaller proteins may be able to permeate the membrane but their motion should be retarded. Even if some protein does permeate the membrane, the concentration in the dialysis fluid should be at a significantly lower concentration than in the bulk which will extend the performance lifetime of a biosensor. Future work needs to be performed to evaluate the size exclusion effect of the microdialysis membrane on larger molecular weight proteins such as albumin and insulin.

Permeable polysilicon membranes should have faster mass transfer rates and better filtration capabilities than diffusion channels since they are a very thin membrane with smaller pores, and a greater surface area for diffusion to occur over. The smaller pore sizes will more effectively retard large MW proteins. However, the thin membranes also make them extremely fragile, which may perclude them from being effectively used. Future work will focus on determining how larger molecules such as serum proteins permeate a microdialysis membrane to allow optimization of the design. This will allow a balance between mass transfer rates and filtering effectivness of a membrane.

In order to fluidically couple the microdialysis microneedle to the analysis chip, a seat was defined by DRIE and the needle was placed into it. The needle was then set using a two part epoxy. Fluid was infused through the needle using a syringe to verify that nonleaking interconnection was achieved. Afterwards, the needle was placed in a concentrated fluorescein solution for a half hour to allow material to equilibrate across the membrane. The fluid was then forced out of the needle with a syringe and the flow on the microchip was recorded to video. An upper and lower channel can be seen. The top channel exits the microchip into the microneedle. The bottom channel shows fluid which has exited the needle back into the chip. The fluid entering and exiting the microneedle after it was allowed to equilibrate in a fluorescein solution is shown

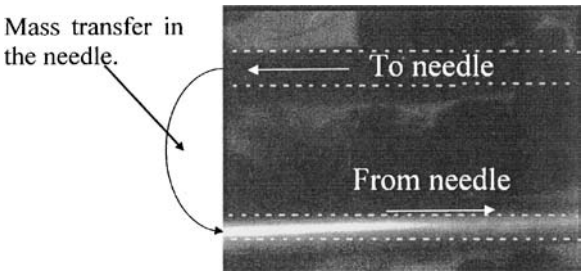

Fig. 14. *Two microchannels with flow entering and leaving the microdialysis needle after fluorescein dye has equilibrated across the dialysis membrane in the microneedle. The channels are delineated by the dashed white lines. The needle is not seen in the frame but forms a continuous fluid channel to the left of the frame.*

in Figure 14. The fluid exiting the needle is highly fluorescent showing the material flux across the microdialysis membrane. Since there was no dye in the solution which was infused into the needle from the flow channel, the dye had to diffuse into the needle from the fluorescein solution on the outside. This demonstrates the ability to use microdialysis needles to sample biological solutions by allowing compounds to equilibrate across the membrane into a dialysis fluid. The fluid can then be pumped downstream to a on-chip sensor for analysis of the solution.

Based on estimates, it will take about 15 seconds for analytes to equilibrate through the microdialysis needle. At a flow rate of 1 nl/s, less than 100 μ1 of dialysis fluid will be consumed after 24 hours of continuous operation. A flow rate of 1 nl/s will ensure that the dialysis fluid will equilibrate with interstitial fluid. Figures 9–11 indicate that at 1 nl/s the fluid only needs to travel only 300 μm down the passage before it is at equilibrium. Since the flow passages designed are 4 mm long, the fluid should have more than sufficient residence time to come to equilibrium.

As with all microneedles, strength and robustness are the major factors in determining the range of their applications. These microdialysis needles must be able to tolerate forces associated with insertion, intact removal and normal human movements if they are to be integrated into portable biomedical devices. Silicon based microneedles are strong and can easily pierce the skin but they are also brittle materials which fracture. In addition, the polysilicon microdialysis membrane needs to remain intact as a microshell on top of the silicon base. Based upon beam and plate theory the base should be able to support about 2 Newtons in bending and 0.14 N before buckling. The polysilicon membrane should be able to support a stress of 2666 KPa without failure. Therefore it can be concluded that the probable failure mode of the microdialysis needles will be buckling or bending fracture during insertion and not due to a high fluid pressure shattering the supported membranes.

Since the needle volume is only 2.6 n1, a flow rate of 1 nl/s could be very quickly moved onto a planar electrochemical sensor and continuous real time monitoring could be performed, with only a few seconds delay between the fluid sampling and sensing. Microdialysis microneedles are an attractive first step in maximizing the efficiency of portable medical monitors by decreasing size, patient discomfort, fluid volumes, and therefore energy consumed by the device.

Acknowledgments

The authors would like to thank Ron Wilson for his help with SEM pictures. All devices were fabricated in the Berkeley Microfabrication Center.

This work has been supported by a grant from the Becton Dickinson Technology Center managed by Dr. Noel Harvey and by DARPA through the Composite CAD program managed by Dr. Anantha Krishnan.

References

J. Brazzle, I. Papautsky, and A.B. Frazier, IEEE Engineering in Medicine and Biology Magazine, IEEE **18**(6) 53–58 (1999).

T.A. Desai, W.H. Chu, J.K. Tu, G.M. Beattie, A. Hayek, and M. Ferrari, Biotechnology and Bioengineering **57**(N1), 118–120 (1998).

T.A. Desai, D. Hansford, and M. Ferrari, Journal of Membrane Science **159**(N1–2), 221–231 (1999).

S. Henry, D.V. McAllister, M. Allen, and M. Prausnitz, in *Proceedings of the IEEE Eleventh Annual International Workshop on MEMS* (Heidelberg, Germany, 1998), pp. 494–498.

M. Lambrechts and W. Sansen, *Biosensors: Microelectrolchemical Devices* (The Institute of Physics Publishing, New York, NY, 1992).

K. Lebouitz, "MEMS microshells for microneedles, microscale fluid visualization, and vacuum packaging of microdevices," University of California at Berkeley, Ph.D. Thesis, 1998.

D. Liepmann, A. Pisano, and B. Sage, Diabetes Technology & Therapeutics **14**, 469–476 (1999).

D. Liepmann, B.H. Sage, A.P. Pisano, and R.T. Howe, "Integrated μ FLUME Reconstitution System for Biological and Medical Supplies," Abstract to DARPA, February 1997.

L. Lin, A.P. Pisano, and R.S. Muller, in *Solid State Sensors and Actuator Conference, Transducers '93* (Japan, 1993), pp. 237–240.

E.M. Renkin, Journal of General Physiology **41**, 225–243 (1954).

N. Talbot and A.P. Pisano, in *Proceedings 1998 Solid State Sensor and Actuator Workshop* (Hilton Head S.C., 1998), pp. 265–268.

B.C. Towe and V.B. Pizziconi, Biosensors and Bioelectronics (Elsevier) **12**(9/10), 893–899 (1997).

J.D. Zahn, N.H. Talbot, D. Liepmann, and A.P. Pisano, Biomedical Microdevices **2**(4), 295–303 (2000).